Measurement of Temperature, Density, and Particle Transport with Localized Dopants in Wire-Array *Z* Pinches

B. Jones,[1,*] C. Deeney,[1] J. L. McKenney,[1] D. J. Ampleford,[1] C. A. Coverdale,[1] P. D. LePell,[2] K. P. Shelton,[2] A. S. Safronova,[3] V. L. Kantsyrev,[3] G. Osborne,[3] V. I. Sotnikov,[3] V. V. Ivanov,[3] D. Fedin,[3] V. Nalajala,[3] F. Yilmaz,[3] and I. Shrestha[3]

[1]*Sandia National Laboratories, Albuquerque, New Mexico 87185, USA*
[2]*Ktech Corp., Albuquerque, New Mexico 87123, USA*
[3]*University of Nevada, Reno, Nevada 89557, USA*

(Received 15 September 2006; published 11 March 2008)

Axially localized NaF dopants are coated onto Al cylindrical wire arrays in order to act as spectroscopic tracers in the stagnated *z*-pinch plasma. Non-local-thermodynamic-equilibrium kinetic models fit to Na *K*-shell lines provide an independent measurement of the density and temperature that is consistent with spectroscopic analysis of *K*-shell emissions from Al and an alloyed Mg dopant. Axial transport of the Na dopant is observed, enabling quantitative study of instabilities in dense *z*-pinch plasmas.

DOI: 10.1103/PhysRevLett.100.105003 PACS numbers: 52.59.Qy, 52.25.Fi, 52.58.Lq, 52.70.La

Wire array *z* pinches are intense soft x-ray sources, presently capable of producing up to 250 TW and 1.8 MJ of radiation [1] from a 200 eV blackbody [2], high-atomic-number (*Z*) tungsten plasma for inertial confinement fusion studies [3]. Low- to mid-*Z* wire arrays (Al to Cu on existing accelerators) are designed for *K*-shell x-ray production at electron temperatures (T_e) up to 4 keV [4]. These loads provide an opportunity for x-ray spectroscopic study of plasma properties and radiation physics in the high-energy-density stagnated column created after the imploding cylindrical plasma reaches the central axis. Spatial structure coupled with radiation transport make all pinches very challenging to diagnose [5,6].

Three-dimensional (3D) structure can significantly impact energy deposition in the *z*-pinch plasma. In addition to millimeter-scale magnetohydrodynamic (MHD) instabilities [7] appearing during the wire ablation and implosion phases, 10–100 μm structures may be present [8,9]. Turbulence has been invoked in one-dimensional (1D) MHD *z*-pinch simulations to account for 3D effects and match experimentally observed plasma diameters [10]. The impact of turbulence on compressibility and heating could be significant for all classes of *z* pinches.

Insight into plasma energy balance and instabilities has been previously obtained in magnetically confined toroidal plasmas by exploiting the relationships between energy and particle transport through the use of spectroscopic techniques [11]. Perturbative injection of dopants at the plasma edge [12] offers a particularly powerful approach to transport studies. Similar techniques employing *K*-shell spectroscopy of low- to mid-*Z* (e.g., NaF) localized dopants have been employed in laser-driven experiments for transport studies [13] and diagnosis of plasma temperature and density [14,15].

In this Letter, the technique of using localized spectroscopic dopants for plasma characterization and transport analysis is extended to wire-array *z*-pinches by coating millimeter-length NaF bands onto the wires. Coatings have been previously deposited over the entire length of wire arrays to modify the plasma opacity and increase *K*-shell yields [16]. In the present work, the localized coating minimally perturbs the dynamics and acts as a diagnostic tracer, enabling a study of material transport in addition to providing an independent measurement of the plasma parameters. As this technique is extended to higher current (hence higher mass) implosions, low-mass dopants can be used to minimize opacity effects.

Cylindrical arrays of eight 15 μm diameter Al 5056 (5% Mg) wires with 16 mm array diameter and 20 mm height were fielded on the 1 MA, 100 ns rise-time Zebra generator [17]; these loads have been discussed in detail in Refs. [18,19]. Physical vapor deposition was used to coat NaF thicknesses of 1400 or 2800 Å, corresponding locally to 5% or 8% of the wire mass per unit length. The wires were mounted in racks [20] during this process and coated on both sides with masking near the wire controlling the axial extent of the dopant. The dopants were deposited in a fixed position relative to a weight crimped onto one end of the wire which was then held at the top of the load hardware so that the dopants on all wires in the array were aligned axially. The alignment technique was verified to ± 200 μm by hanging wires with thick Au test coatings that were readily visible by eye. In these experiments on Zebra, the presence of the NaF dopant is observed not to impact the implosion dynamics via laser shadowgraphy, gated x-ray pinhole imaging, and x-ray power and yield diagnostics (x-ray output is dominated by $\pm 10\%$ shot-to-shot variation with or without the dopant).

K-shell spectra were obtained with convex KAP crystal spectrometers [21] over 1–4 keV photon energies with $\lambda/\Delta\lambda \sim 300$ spectral resolution. Slit imaging provided 1D spatial resolution in the axial and radial directions

(two separate instruments) in order to study dopant transport. Time-integrated exposures were collected with either Kodak DEF or Biomax MS film [22], and provide an initial assessment of the transport, though time-resolved data are certainly desired in future work.

Figure 1(a) shows a radially resolved spectrum, in which Na Ly-α and He-α emission lines [labeled in Fig. 1(c)] are seen only in the core of the z pinch. Radial lineouts of line exposures have 1.2 mm FWHM (the 0.5 mm slit provides 1.3 mm geometric spatial resolution which limits this measurement). This is consistent with the coating ablating and streaming to the array axis early in time and remaining in the core of the stagnated column while the imploding Al and Mg exhibit line emission at larger radii. An axially resolved spectrum in Fig. 1(b) shows the Na dopant lines fairly localized (but longer than their initial 1 mm extent) in the stagnated z pinch centered near their initial axial position at $z = 0$ (the anode is positioned at the top of the image and the cathode at the bottom). These data were obtained with a 1 mm slit to augment the Na exposure. Spectra from identical wire arrays without the NaF dopant are very similar, but with the Na lines absent. It should be noted that the Mg lines extend axially throughout the pinch

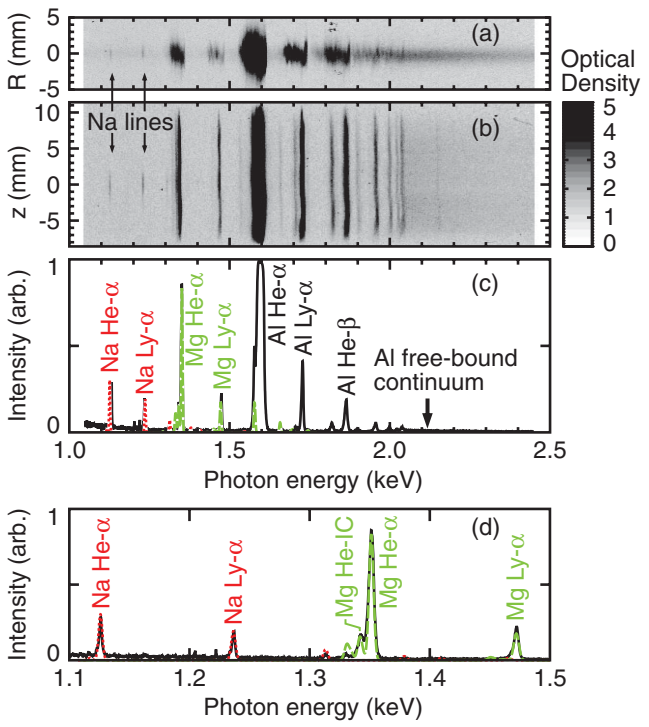

FIG. 1 (color). (a) Radially and (b) axially resolved, time-integrated spectra from Zebra shot 363 showing Na K-shell line emission from the core of the z-pinch plasma, centered at the initial dopant position $z = 0$. (c) A spectral lineout of (b) across the center of the Na lines, corrected for film response and filter transmission, is fitted with non-LTE kinetic models of Na (dotted red line) and Mg (dashed green line), both inferring $T_e \approx 280$ eV, $n_e \approx 2 \times 10^{20}$ cm^{-3}, and $Z \approx 10$. (d) Expanded view of (c).

indicating that the plasma is hot enough to radiate from the K shell along its entire length. Consequently, we infer that variation in Na line emission corresponds to variation in Na density rather than electron temperature.

Combined with non-LTE kinetic modeling, the Na line emission provides an independent measurement of the stagnated plasma parameters which can be compared with results inferred from the Mg line emission. Figure 1(c) shows a lineout of Fig. 1(b) centered on the Na lines ($z = 0$). Al He-α is expected to be significantly opaque (and is saturated here), but emission is assumed to be optically thin from the 5% Na and Mg dopants. Two non-LTE kinetic models have been used in this work. The Mg model was developed to describe K-shell radiation from implosions of X pinches and wire arrays with Al 5056 wires [23]. The Na model was developed to describe K-shell spectra from wire arrays coated with NaF. Both models include all ionization stages with a detailed structure, in particular, singly excited states of H-like ions up to $n = 6$ for Mg and $n = 5$ for Na, He-like ions up to $n = 5$, and Li-like ions up to $n = 4$. Energy level structures and complete radiative and collisional coupling data were calculated by the FAC code [24]. Separately simulated x-ray spectra of Na and Mg K-shell emissions are shown overlayed on the experimental data in Fig. 1(c), and represent best fits to the data. Line ratios of He-α to Ly-α are particularly sensitive to T_e while line ratios of the He-like intercombination (IC) line to He-α resonance line are sensitive to the electron density n_e, so this analysis constrains these values with error bars of ± 25 eV and a factor of 2, respectively, with error in effective charge Z of 2%. The Na spectral fit indicates $T_e = 270$ eV, $n_e = 2 \times 10^{20}$ cm^{-3}, and $Z = 9.6$, while the Mg fit gives reasonable agreement with $T_e = 290$ eV, $n_e = 2 \times 10^{20}$ cm^{-3}, and $Z = 10.3$. A least-squares fit of the form $\exp(-h\nu/kT_e)$ (plus a film background offset) to the Al free-bound continuum in Fig. 1(b) and 1(c) between 2.1–3.5 keV gives $T_e = 290 \pm 10$ eV, also in agreement.

This analysis validates the concept of using a localized, low-mass, minimally perturbative dopant to diagnose plasma parameters in wire array z pinches independent of wire material. Nested Al array interpenetration has previously been diagnosed by placing 5% Mg dopant (i.e., Al 5056) in only one of the two arrays [25], but the coating approach potentially can be applied to any wire material regardless of alloy availability, perhaps providing a path to diagnosis of plasma parameters in a tungsten z pinch via low-Z dopant K-shell spectroscopy. It may also be possible to imbed tracers in wires by overcoating the entire wire length in order to study ablation dynamics and modify the radial position of the dopant in the imploding plasma.

In investigating axial particle transport of the localized dopant, a 0.5 mm slit was used to provide 1.3 mm spatial resolution. Axial lineouts capturing the time-integrated Na He-α line exposure (corrected for film response) from several Zebra shots are shown in Fig. 2, demonstrating that the axial spread of the material exceeds the signal

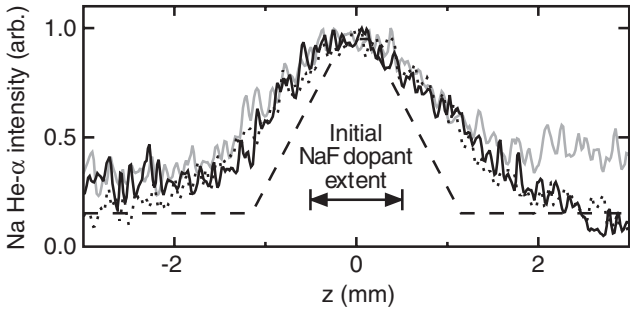

FIG. 2. Axial lineouts of Na He-α emission from Zebra shots 424 (solid black line), 426 (gray line), and 427 (dotted line) show axial particle transport beyond the initial NaF dopant position smoothed by the spatial resolution of the instrument (dashed line).

expected from Na remaining at its initial position but smoothed by the 1.3 mm instrumental resolution (dashed line). Asymmetries seen in the wings of the axial profiles are real but vary from shot to shot, so we will focus only on the spread of the main peak around $z = 0$.

Possible particle transport mechanisms that could result in the observed spread include axial flow as material is ablated from the wires [26], thermal expansion as ablated material streams toward the axis, turbulence in the precursor [9], MHD instability convection, or turbulence in the stagnated pinch. In order to quantify the level of transport observed for comparison with potential mechanisms, we consider the function

$$n(z) = \frac{n_0}{2}\left[\mathrm{erf}\left(\frac{z + L/2}{\sigma}\right) - \mathrm{erf}\left(\frac{z - L/2}{\sigma}\right)\right], \qquad (1)$$

which is the solution to the 1D Vlasov equation for thermal free expansion (in the presence of a neutralizing electron background) of the Na density profile along the axial z direction for a dopant of initial length L and a free-space boundary condition. It is also the free-space solution to the 1D diffusion equation $\partial n/\partial t = D\partial^2 n/\partial z^2$. The parameter σ is the scale length for transport of material, and is given by $\sigma = \sqrt{2}v_{\mathrm{th},i}t = t\sqrt{2T_i/m_i}$ for the case of thermal expansion which we will consider during the ablation phase, or $\sigma = \sqrt{4Dt}$ for diffusive transport in the dense plasma column.

Figure 3(a) shows Eq. (1) plotted for various values of σ with $L = 1$ mm; for low values the density profile is stepped, and it spreads into a broader Gaussian as σ increases. With only time-integrated spectra available, we cannot resolve the time scale of transport more accurately than the length of the x-ray pulse, but we can use data as in Fig. 2 to constrain σ. Figure 3(b) shows the axial profile of Na Ly-α emission (gray line) from dopant of 1 mm initial length (dotted line). As emissivity is proportional to the square of density in the optically thin limit, a function of the form $an^2(z - b) + c$ (which is also smoothed corresponding to the 1.3 mm spatial resolution) is fit to the data. Here n is from Eq. (1) and a, b, and c are scale factor, peak

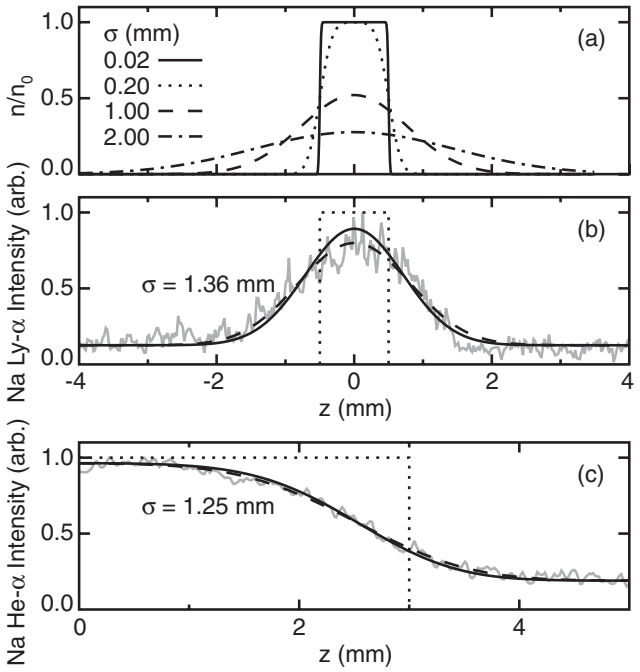

FIG. 3. (a) Evolution of an initially 1-mm-long band at $z = 0$ for various values of σ per Eq. (1). (b) A fit (dashed line) including smoothing for instrumental spatial resolution to the time-integrated Na Ly-α axial lineout from Zebra shot 363 (gray line), with a 1-mm-long NaF band coated at $z = 0$ (dotted line). A solid line shows the corresponding intensity profile without instrumental spatial resolution broadening. (c) A similar fit to the edge of a long dopant band from shot 454 also shows particle transport.

offset, and film background fit parameters, respectively. The fit (dashed line) is sensitive to the width of the spread in the profile. The function is also plotted without smoothing for spatial resolution (solid line), which is a minor correction. The nonlinear least-squares fit yields $\sigma =$ 1.36 mm, and similar values are obtained in experiments observing particle transport at the edge of a long dopant band [Fig. 3(c)] where diffusion has softened the edge of the sodium tracer. From a total of six shots (with both long and short bands), the average σ is 1.6 mm, with a standard deviation of $\pm 17\%$ (shot-to-shot variation), an average spread of $\pm 26\%$ in the fits to Na He-α and Ly-α for a given shot, an average 2% fit error, and a $+0\%/-30\%$ error due to worst case dopant misalignment between wires. The analysis constrains σ to the range 0.9–2.1 mm for this load.

Axial flow in the corona surrounding the dense wire core [26] could lead to as much spread as $\sigma = 0.5$ mm, the wavelength of the natural ablation nonuniformity [27]. Assuming ablated plasma with temperature $T_i = T_e =$ 40 eV [27] and using $t = 60$ ns, the time from the start of current to the formation of the precursor in the Zebra experiments, we can estimate $\sigma = t\sqrt{2T_i/m_i} \sim 1.2$ mm. Thus, thermal expansion of the ablated Na on its way to the axis might explain the observed transport, or at least con-

tribute to the spread. We note, though, that this is an upper bound as the plasma may well be collisional during its evolution.

We can also consider collisional diffusion in the hot, stagnated z pinch with parameters as determined from spectroscopy and assuming electron-ion equilibration, i.e. $T_i = T_e = 280$ eV, $n_e = 2 \times 10^{20}$ cm^{-3}, $Z = 10$, and $n_i = n_e/Z$. From a random walk argument where colliding particles of mass m_i make a step Δz in a time Δt, the collisional ion diffusion coefficient is

$$D \sim \frac{\Delta z^2}{\Delta t} \sim \nu_{ii} \lambda_{mfp,i}^2 \sim \frac{v_{\mathrm{th},i}^2}{\nu_{ii}} \sim \frac{T_i}{m_i \nu_{ii}} \sim \frac{12\pi^{3/2}\epsilon_0^2 T_i^{5/2}}{m_i^{1/2} n_i Z^4 e^4 \ln\Lambda}. \quad (2)$$

The ion mean free path is estimated as $\lambda_{mfp,i} \approx 30$ nm and the collision time is $1/\nu_{ii} \approx 1$ ps, consistent with the application of a diffusion equation to the stagnated plasma. Assuming that the diffusion time scale is on the order of the x-ray power FWHM $t \sim 40$ ns (for both total and K shell), Eq. (2) gives $\sigma = \sqrt{4Dt} \sim 10$ μm, well short of the experimental result. The experimental value of σ can be matched by taking $T_i = 15$ keV, which corresponds to equating the ion thermal velocity $v_{\mathrm{th},i}$ with the 25 cm/μs thin-shell (0D) calculated implosion velocity. Such an ion temperature is not unreasonable, but would be thermalized on a subnanosecond time scale rather than persisting for 40 ns. Transport could also be caused by MHD convection in the nonuniform implosion or by microscale turbulence, leading to a larger effective D. Future time- and space-resolved spectroscopy will be required to observe when the transport occurs and to distinguish conclusively between these mechanisms.

In summary, localized spectroscopic dopants provide a promising approach for measuring plasma parameters and transport properties in wire array z pinches. The low-mass NaF coatings employed do not perturb the implosion by a detectable amount, but produce enough line emission to allow inference of temperature and density via K-shell spectroscopy coupled with non-LTE kinetic modeling. Dopants can potentially be applied to any wire-array material, perhaps including high-Z tungsten wires for which spectroscopic diagnosis is otherwise difficult.

The localized nature of the coatings used also allows for measurements of particle transport. Values of σ from the analysis presented here demonstrate that particle transport is observable, establishing a path for quantitative study. Time- and space-resolved measurements will be valuable in future experiments to assess at what stage in the z-pinch implosion the transport occurs. Experimental measurements of particle transport may help to constrain proposed z-pinch instability mechanisms, and to benchmark codes including subgrid or phenomenological turbulence models, or 3D MHD convection. Localized dopants may also be used to track bulk material flow in noncylindrical geometries, such as conical and radial wire arrays which generate directed jets in laboratory astrophysical studies [28].

The authors would like to thank the Materials Processing and Coatings Laboratory, Albuquerque, NM for manufacturing wires for this work; A. L. Astanovitskiy, B. Le Galloudec, S. Batie and the University of Nevada, Reno (UNR) Zebra team for supporting the experiments; and T. E. Cowan (UNR), J. P. Chittenden (Imperial College), A. A. Esaulov (UNR), and B. V. Oliver (Sandia) for valuable interactions. Sandia is a multiprogram laboratory operated by Sandia Corporation, a Lockheed Martin Company, for the US DOE's National Nuclear Security Administration under Contract No. DE-AC04-94AL85000. Work at UNR's Nevada Terawatt Facility is supported by DOE/NNSA Grant No. DE-FC52-01NV14050.

*bmjones@sandia.gov

[1] C. Deeney *et al.*, Phys. Rev. Lett. **81**, 4883 (1998).
[2] M. E. Cuneo *et al.*, Phys. Plasmas **8**, 2257 (2001).
[3] M. K. Matzen *et al.*, Phys. Plasmas **12**, 055503 (2005).
[4] B. Jones *et al.*, J. Quant. Spectrosc. Radiat. Transfer **99**, 341 (2006).
[5] J. P. Apruzese *et al.*, Phys. Plasmas **8**, 3799 (2001).
[6] L. Gregorian *et al.*, Phys. Rev. E **71**, 056402 (2005).
[7] J. P. Chittenden *et al.*, Plasma Phys. Controlled Fusion **46**, B457 (2004).
[8] M. G. Haines *et al.*, Phys. Rev. Lett. **96**, 075003 (2006).
[9] V. I. Sotnikov *et al.*, IEEE Trans. Plasma Sci. **34**, 2239 (2006).
[10] J. W. Thornhill *et al.*, Phys. Plasmas **1**, 321 (1994).
[11] N. J. Peacock, Astrophys. Space Sci. **237**, 341 (1996).
[12] E. J. Synakowski *et al.*, Phys. Rev. Lett. **65**, 2255 (1990).
[13] Y. Al-Hadithi *et al.*, Phys. Plasmas **1**, 1279 (1994).
[14] K. B. Fournier *et al.*, J. Quant. Spectrosc. Radiat. Transfer **71**, 339 (2001).
[15] C. A. Back, D. H. Kalantar, and R. L. Kauffman, Phys. Rev. Lett. **77**, 4350 (1996).
[16] C. Deeney *et al.*, Phys. Rev. E **51**, 4823 (1995).
[17] B. S. Bauer *et al.*, AIP Conf. Proc. **409**, 153 (1997).
[18] V. V. Ivanov *et al.*, Phys. Plasmas **13**, 012704 (2006).
[19] V. L. Kantsyrev *et al.*, IEEE Trans. Plasma Sci. **34**, 194 (2006).
[20] B. Jones *et al.*, Rev. Sci. Instrum. **75**, 5030 (2004).
[21] T. Nash *et al.*, Rev. Sci. Instrum. **70**, 302 (1999).
[22] K. M. Chandler *et al.*, Rev. Sci. Instrum. **76**, 113111 (2005).
[23] A. Safronova *et al.*, AIP Conf. Proc. **808**, 149 (2006).
[24] M. F. Gu, AIP Conf. Proc. **730**, 127 (2004).
[25] C. Deeney *et al.*, Phys. Rev. Lett. **93**, 155001 (2004).
[26] C. J. Garasi *et al.*, Phys. Plasmas **11**, 2729 (2004).
[27] S. V. Lebedev *et al.*, Laser Part. Beams **19**, 355 (2001).
[28] S. V. Lebedev *et al.*, Plasma Phys. Controlled Fusion **47**, B465 (2005).